1988

Scatterer Discrimination Based Upon Natural Resonance Annihilation

Morgan, M.A.

Journal of Electromagnetic Waves and Applications, Vol. 2, No. 5/6, pp. 481-502, 1988

http://hdl.handle.net/10945/46788

Journal of Electromagnetic Waves and Applications, Vol. 2, No. 5/6, 481–502, 1988

Scatterer Discrimination Based Upon Natural Resonance Annihilation

M. A. Morgan

Electrical & Computer Engineering Department
Naval Postgraduate School
Monterey, CA 93943, USA

Abstract– Classification of electromagnetic scatterers by the annihilation of natural modes is considered. After providing some historical background, the conceptual basis of this methodology is discussed, followed by a development of the requisite theoretical techniques. Implementations of some resonance annihilation schemes are illustrated and resultant validations using synthetic signals, integral equation computations and scattering measurements are featured.

HISTORICAL BACKGROUND

The concept of radar target identification by use of electromagnetic natural resonances was introduced in 1974 by Mains and Moffatt [1]. This idea, in turn, evolved from the earlier work of Baum at the Air Force Weapons Laboratory [2], who developed the formalism known as the Singularity Expansion Method (SEM) for use in the analysis of nuclear EMP vulnerability of strategic systems. Within the context of SEM, the response of a system can be represented as a weighted expansion of complex natural modes. These modes, which are self-sustaining in the absence of any excitation, are functions of the structural geometry and composition of the scatterer and are independent of the incident excitation. The temporal variation of each mode-pair has the form of an exponentially decaying sinusoid. In the Laplace transform domain these natural resonances are represented by pairs of conjugate poles in the left-half complex plane. The knowledge of a finite subset of these poles for each potentially observable target can thus serve as an aspect-invariant parameter set for scatterer identification.

In an early paper by Tesche [3], it was noted that the SEM Heaviside expansion in the Laplace domain for the response of a thin-wire antenna needed to be augmented by an s-plane entire-function. Theoretical studies by Morgan [4], and Pearson [5], have since shown that the SEM pole-series expansion is a complete description of the scattered signal only in the late-time. This portion of the scattered field is due to the undriven currents that remain *after* the incident field has completed its illumination of the target, and is termed the "late-time". The "early-time" scattering response is due to induced currents that result, in part, from the incident field illumination.

Much of the initial work in utilizing natural resonances for non-cooperative target recognition (NCTR) has been in the context of attempting to identify

the dominant poles in the time-domain scattering responses of simple targets. Early efforts towards demonstrating the feasibility of natural resonance NCTR were disappointing. These failures resulted from both the high noise sensitivity inherent in pole extraction algorithms, [6], and because attempts were made to process the entire scattered signal rather than just the undriven late-time portion.

A new class of techniques has arisen for aspect-independent NCTR which is based upon the selective annihilation of resonances in the received scattered signal. These methods are extensions of the original "K-Pulse" concept proposed by Kennaugh [7]. Independent efforts by Morgan [8] and Chen [9] have shown that resonance annihilation NCTR has two primary advantages versus NCTR which utilizes pole extraction: identifications using SNR's in the range of 10 dB and, secondly, orders of magnitude reduction in signal processing time.

NATURAL RESONANCE SCATTERING

Consider the transient electromagnetic scattering problem as depicted in Fig. 1, wherein a perfectly conducting finite-sized object is being illuminated by a generalized incident field in free space. The induced current on the surface of the object will satisfy the magnetic field integral equation (MFIE), [10],

$$\overline{J}(\overline{r},t) = 2\hat{n} \times \overline{H}^i(\overline{r},t) + \iint_{S_{PV}} \overline{\overline{K}}(\overline{r},\overline{r}',t) \cdot \overline{J}(\overline{r},t-|\overline{r}-\overline{r}'|/c)\, dS \qquad (1)$$

where $\hat{n}$ is the outward (to the surface) unit normal vector, $\overline{J}$ is the surface current density, $\overline{H}^i$ is the incident magnetic field at the surface, $\overline{\overline{K}}$ is a dyadic Green's function kernel and the principal-value (PV) type integral excludes the point $\overline{r} = \overline{r}'$. The cross product of $\hat{n}$ and the incident magnetic field forms the physical optics portion of the induced current while the surface integral term provides the "feedback" current to each point on the scatterer due to all other induced current values.

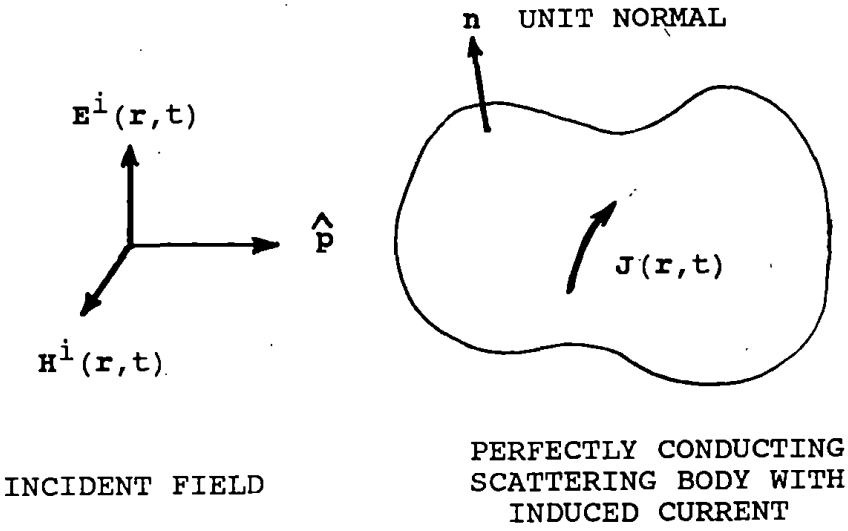

Figure 1. Transient electromagnetic scattering.

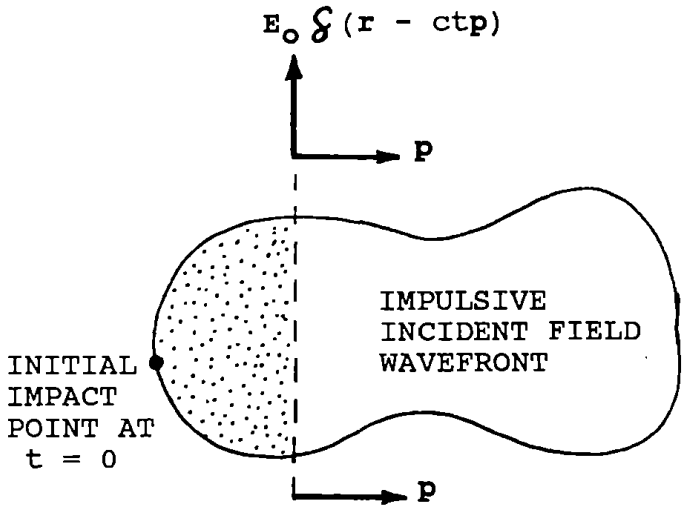

Figure 2. Plane wave impulse illumination.

With $\overline{H}^i = 0$, the solutions of (1) are termed the natural modes of the scattering problem. These source-free current modes are of the form $\overline{J}_n(\overline{r}) \cdot \exp(s_n t)$, where the natural resonance frequencies, $s_n = \sigma_n + j\omega_n$, are functions of the physical structure and composition of the scatterer. Furthermore, the resonances appear in complex conjugate pairs in the left-half s–plane and can be discretely indexed for the case of finite 3–D conducting scatterers, [11]. Although there are an infinite number of natural resonance modes for even the simplest object, only a limited subset of these will be substantially excited by an incident field having a finite practical bandwidth.

The scattered field due to an incident plane wave will be composed of two parts: an early-time driven response and a late-time natural mode response. This result can be explained by considering the application of (1) to the situation depicted in Fig. 2. Note that the *impulsive* plane wave incident field will be identically zero everywhere on the surface of the scatterer except on the conformal ring which circumscribes the surface at the intersection with the plane wavefront, as indicated by the dashed line. This conforming source ring on the scatterer's surface changes cross-sectional shape and position as the wavefront moves over the scatterer at the velocity of light. From (1), the surface current at points on the wavefront ring will be composed of the physical optics term, $2\hat{n} \times \overline{H}^i$, added to a Green's function integral contribution from all previously illuminated points on the scatterer. These points, which reside in the wake of the incident field, are dot-shaded in Fig. 2. Because of causality, there is no induced current at points on the scatterer which are ahead of the incident wavefront.

Let us now consider the resultant back-scattered far-field (in the direction $-\hat{p}$ at a very large distance) due to the surface current distribution. This echo field will be due to a non-PV type far-field Green's function surface integration having

the form, [10],

$$\overline{H}^s(-r\hat{p},t) = \frac{1}{4\pi cr}\frac{\partial}{\partial t}\iint_S \hat{p}\times\overline{J}(\overline{r}',t-|\overline{r}-\overline{r}'|/c)\,dS' \tag{2}$$

Upon substituting (1) into (2), two distinct terms emerge: the physical optics scattered field generated by the $2\hat{n}\times\overline{H}^i$ driven current and the scattered field produced by the source-free wake current behind the incident wavefront. The physical optics scattered field can be shown to be directly proportional to the second time derivative of the projected silhouette area of the scatterer in the incident direction, $\hat{p}$, and is thus highly *aspect dependent*, [12]. The remainder of the scattered field is due to a locally source-free current distribution on a time-varying portion of the surface in the wake of the incident impulse. As is shown in [4], this wake current can be represented by a Class 1 SEM expansion, having constant coefficients. However, because the surface area is changing in (2), wherein the wake current integration takes place, the resultant scattered field will contain the same exponential resonance terms as the source free current, but with *time-varying* coefficients until such time as the scattered field results from a complete surface integration. This form of the SEM expansion is termed "Class 2". The backscattered far-field is

$$\overline{H}^s(-r\hat{p},t) = u(t-r/c)\left\{\overline{H}_{po}(-r\hat{p},t)+\sum_{\substack{n=-\infty\\ n\neq 0}}^{\infty}\overline{H}_n(-r\hat{p},t)\exp(s_nt)\right\} \tag{3}$$

where the time-varying vector-residues, $\overline{H}_n$ become constant after a delay of $2D/c$ from the initial scattered field turn-on. In this equation, D is the length of the scattering object in the direction parallel to $\hat{p}$. At this same transition instant, in going from the class 1 to the class 2 SEM forms, the physical optics field vanishes and there remains only the constant coefficient expansion. The early-time scattered field is thus composed of both a physical optics term and a class 2 SEM expansion, with time-varying coefficients, while the late-time field can be represented by a simple class 1 expansion.

The general case of bistatic scattering at any distance (not necessarily in the far-field) has been considered in [4]. If $\overline{r}$ is used to represent a particular scattered field point and $\overline{r}'$ is used to denote points on the surface of the scatterer, then the time at which the physical optics field reaches $\overline{r}$ from $\overline{r}'$ will be

$$t_{po} = \left[\hat{p}\cdot\overline{r}' + \left|\overline{r}-\overline{r}'\right|\right]/c \tag{4}$$

By allowing $\overline{r}'$ to vary over the surface, one can define the minimum and maximum of t_{po}. The early-time field at $\overline{r}$ begins at $t = \min[t_{po}]$ and ends, with transition to the late-time, when $t = \max[t_{po}]$. Two special far-field cases result from this analysis: backscattering, as previously considered, and forward scattering, where the early-time duration is of measure zero when the illumination is due to a plane wave impulse. These two cases represent the extrema of possible early-time durations.

Consider now the forms of the natural resonance representations for the general case of an incident plane wave which has time modulation $f(t)$. This $f(t)$ can represent, for example, such radar waveshapes as AM pulsed CW or FM chirp-type waveforms. Assuming that $f(t)$ is time-limited, with duration T, then the resultant time before transition to the late-time in the scattered field will, at all observation points, be lengthened by T vis-a-vis that for the impulse illumination.

THE RESONANCE ANNIHILATION FILTERING CONCEPT

Considering the results of (3), the transient scattered signal waveform will have the generic form,

$$y(t) = \underbrace{y_E(t)\ [u(t) - u(t - T_o)]}_{\text{Early-Time}} + \underbrace{y_L(t)\ u(t - T_o)}_{\text{Late-Time}} + \underbrace{N(t)}_{\text{Noise/Clutter}} \tag{5}$$

The early-time component of this signal is composed of physical optics currents and a class 2 natural mode expansion having time-varying coefficients. The changeover from early to late-time signal components is specified in (5) by the explicit use of unit step functions. For the monostatic scattering case, this transition time is given by

$$T_o = T + 2D/c \quad \text{seconds} \tag{6}$$

where T is the incident pulse width, D is the line-of-sight dimension of the scatterer and c is the velocity of propagation.

The late-time scattering response will be a class 1 natural mode expansion, which can be written using damped sinusoids

$$y_L(t) = \sum_{n=1}^{\infty} A_n \exp(\sigma_n t)\ \cos(\omega_n t + \phi_n) \tag{7}$$

Due to the aspect dependence of the residues, $A_n \exp(j\phi_n)$, modes which are strongly excited at some aspects may essentially vanish at other aspects.

The third component of the received signal is the noise and clutter. This is composed of internal receiver noise and externally generated antenna noise, as well as clutter echoes from scatterers which arrive simultaneously with that of the target. The $N(t)$ is obviously an undesirable element whose presence will increase the difficulty of implementing NCTR using natural resonance annihilation.

The resonance annihilation filter (RAF) concept for NCTR is depicted in Fig. 3. The output of the m-th RAF will be a convolution of its impulse response, $k_m(t)$ with the input signal,

$$z_m(t) = k_m(t) * \Big\{ y_E(t) \Big[u(t) - u(t - T_o) \Big] + y_L(t)\, u(t) + N(t) \Big\} \tag{8}$$

The decision process for NCTR is based upon selecting that target whose RAF output exhibits the lowest late-time signal energy,

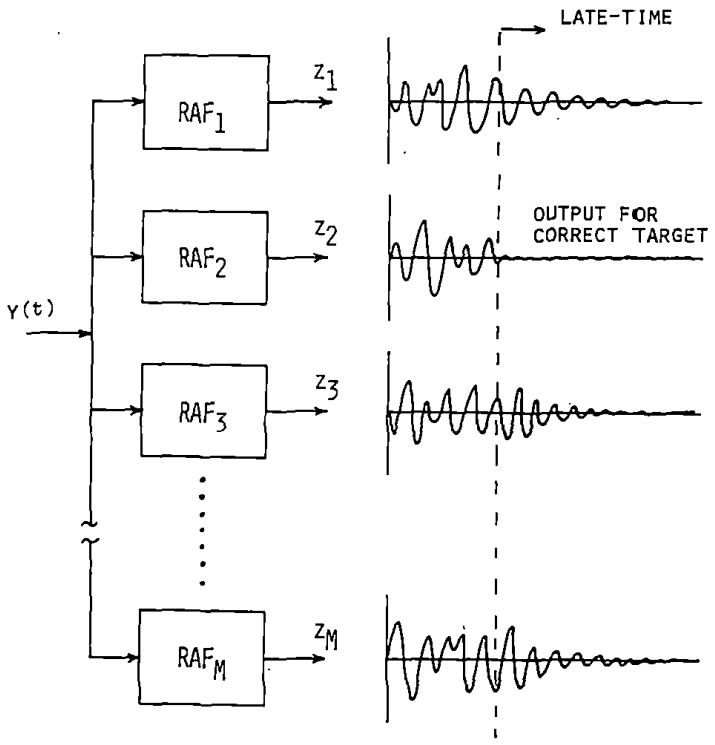

Figure 3. RAF identification process

$$\varepsilon_m = \int_{T_L}^{\infty} z_m{}^2(t)\, dt \tag{9}$$

where the late-time startup, T_L, must be large enough to exclude any significant contribution from the convolution with the early-time signal. The RAF is designed to cancel a selected subset of the natural modes, which appear in their pure form only in the late-time. One way to guarantee that there will be no contribution to ε_m from the early-time signal is to use finite impulse response (FIR) digital filters in the design of the RAF's. Such filters are nonrecursive (no feedback paths) and have impulse responses that are identically zero beyond some finite time, T_k, [13]. This would give $T_L > T_o + T_k$ in (9).

Three primary design criteria for RAF's are:

(1) The convolution of the RAF impulse response and the early-time echo signal should decay to an insignificant amplitude in as short a time beyond T_o as is possible. This translates into minimizing the significant duration of the individual impulse responses, T_k.

(2) The ratios of late-time energy for the matched target to that of other targets should be minimized over a range of pertinent aspect angles and polarizations.

(3) The RAF should be designed to minimize the transfer of the pollutant, $N(t)$ through the filter.

The reason for the demand in (1) is to allow a maximum usable late-time interval for computing the energy values in (9). This also assists in optimizing the energy

ratios as discussed for the constraint (2). This first criterion will, however, conflict with that of (3) since effective noise filtering requires either signal integration, through recursive filtering, or by use of extended feed-forward paths in an FIR filter. In either case, there is a tradeoff of the effective RAF impulse response duration for enhanced noise and clutter suppression.

The process is also complicated by the effect on the design of the RAF's when there are uncertainties in the exact pole locations for each target class. This latter sensitivity may be a very real problem where there are multiple variations on the physical configuration of the same type of target.

FILTER EXAMPLES

We are now in a position to consider two RAF examples. The first of these *failed* to consistently provide lower late-time energies for the matched target. As will be shown, this failure resulted from attempts to implement an analog signal processing strategy using digital techniques. The second form of RAF is based entirely upon digital signal processing methods and is shown to be successful using synthetic, integral equation and experimental data. Both of these RAF's are conceptually simple and do not rigorously address the constrained optimization problem which was posed in the previous section. They do, however, provide illustrations of the considerations that must be made and the pitfalls that may appear in even the most elementary implementation methods. Current efforts are underway towards developing optimal RAF designs that more completely address the NCTR constraints.

The first RAF is based upon the use of differential operators to cancel individual natural modes. It follows from elementary calculus that the damped sinusoidal modes in (7) are each a solution of an appropriate first-order homogeneous differential equation having the form

$$L_n\, y_n(t) = (d/dt - s_n)\,(d/dt - s_n^*)\, y_n(t) = 0 \tag{10}$$

where the defined operator, L_n, cancels the n-th mode. Using this simple result, it follows that multiple modes can be annihilated by the successive application of corresponding operators. For example, cancellation of the set of modes $\{y_n(t)\}$, for $n = 1$ to N, requires the use of a $2N$-th order differential operator formed from the product of each L_n in the range indicated. The RAF impulse response is then $k(t) = Lf(t)$, where $f(t)$ is a smoothing function with continuous derivatives up to, and including, order $2N$. It can be shown by using either repeated integration by parts in the time-domain, or Parseval's theorem in the frequency domain, that the convolution obeys

$$k(t) * y(t) = f(t) * L\, y(t) \tag{11}$$

The analytical form of the frequency domain transfer function can be obtained through Fourier transformation of $k(t)$,

$$K(\omega) = \Big\{(j\omega - s_1)\,(j\omega - s_1^*)....(j\omega - s_N)\,(j\omega - s_N^*)\Big\} F(\omega) \tag{12}$$

The inverse transform of the product of $K(\omega)\times Y(\omega)$ is the RAF output waveform. To implement this analytical procedure one might be tempted to make use of a Fast Fourier Transform (FFT) algorithm. The FFT of the sampled $y(t)$ is multiplied at discrete frequency points by the complex-valued analytical $K(\omega)$ in (12). An inverse FFT is then performed to yield the time-series of the RAF output. Aside from usual concerns for aliasing and temporal truncation, which can be managed, there exists a seemingly insurmountable problem with this approach. The $2N$-th order polynomial, which appears within the curly brackets in (12), will tend to provide *extreme* high frequency noise amplification. It was initially believed that a proper $f(t)$ could be found to provide adequate high-frequency compensation. This can be viewed in the time-domain as a smoothing operation on the noise to reduce the effects of high-order differentiations. Use of a Gaussian-shaped smoothing function,

$$f(t) = \exp\left[-\alpha(t - t_0)^2\right] \tag{13}$$

allows the selection of α to provide variable rolloff of $F(\omega)$.

The second form of RAF replaces differential equations for natural mode cancelation with appropriate difference equations. Individual modes in (7) are each solutions to a three-point homogeneous difference equation of the form

$$a_n\, y\left[(p-1)\,\Delta t\right] + y\left[p\Delta t\right] + b_n\, y\left[(p+1)\,\Delta t\right] = 0 \tag{14}$$

where the sampling interval is Δt. The coefficients to cancel the n-th mode-pair are easily found to be

$$\left.\begin{matrix} a_n \\ b_n \end{matrix}\right\} = -0.5\, \exp(\pm\sigma_n \Delta t) \,/\, \cos(\omega_n \Delta t) \tag{15}$$

where the $+$ and $-$ signs in the exponential give, respectively, a_n and b_n. The 3-point difference equation is easily synthesized using a digital FIR filter (also known as a transversal filter). To cancel N pole-pairs, a cascade of N such 3-weight filters can be employed. By combining coefficients that multiply the same sample points, a simpler FIR filter can be generated which has a total of $2N$ delays and $2N + 1$ weights. The difference equation that represents this simplified filter will have the form, [13],

$$z\left[p\,\Delta t\right] = \sum_{m=-N}^{N} C_m\, y\left[(p-m)\,\Delta t\right] \tag{16}$$

This filter is non-causal, but can be implemented for real-time operation by adding N additional time delays. For post-processing of acquired data, as was done in this effort, the filter can be used directly. In the next section, it will be seen that this filter has the same type of high-frequency noise amplification as does the analog differential operator filter. For noisy signals it will thus be necessary to perform additional smoothing on the input signal in the form of a low-pass filter.

RESULTS OF ANNIHILATION FILTERING

The initial tests on both methods were performed using a set of synthetic signals whose late-time form is the sum of damped sinusoids, as in (7). The early-time signal was set equal to

$$y_E(t) = A_o \sin^2(1.5\pi t / T_o) \tag{17}$$

where T_o is the transition-time. The upper half-plane poles and their corresponding residues are shown in Table 1. These values were chosen to simulate the behavior of typical "layered" pole patterns associated with simple symmetrical objects, such as wires and spheres. The constant A_o was selected to provide continuity of the waveform, but not the derivatives, at the transition time, T_o. An $N = 6$ pole-pair synthetic signal is displayed in Figs. 4 and 5, where Gaussian distributed random noise is added in the second case to provide a 10 dB average power SNR.

The testing of the analog-based RAF proceeded only to the the noiseless synthetic signal level, where consistently correct NCTR decisions could *not* be made using this filter type. This set of tests, which was duplicated for the digital FIR RAF with excellent success, involved processing the synthetic signal using multiple versions of the respective RAF. These included an exact six pole-pair filter, as well as "partial" RAF's, which cancelled the first 1, 2 and 4 pole-pairs of the signal, respectively. Additionally, "offset" RAF's, having 1, 2, 4 and 6 pole-pairs, shifted in magnitude by 5% or 10%, were used. These offset RAF's represented alternate targets.

n	Poles		Residues	
	Real	Imag	Magnitude	Phase
1	-0.10	$+j1.50$	10.0	0
2	-0.19	$+j2.85$	7.0	$\pi/2$
3	-0.28	$+j4.20$	5.0	0
4	-0.39	$+j5.85$	3.0	π
5	-0.46	$+j6.90$	2.0	$\pi/2$
6	-0.54	$+j8.10$	1.0	0

Table 1. Synthetic signal poles and residues.

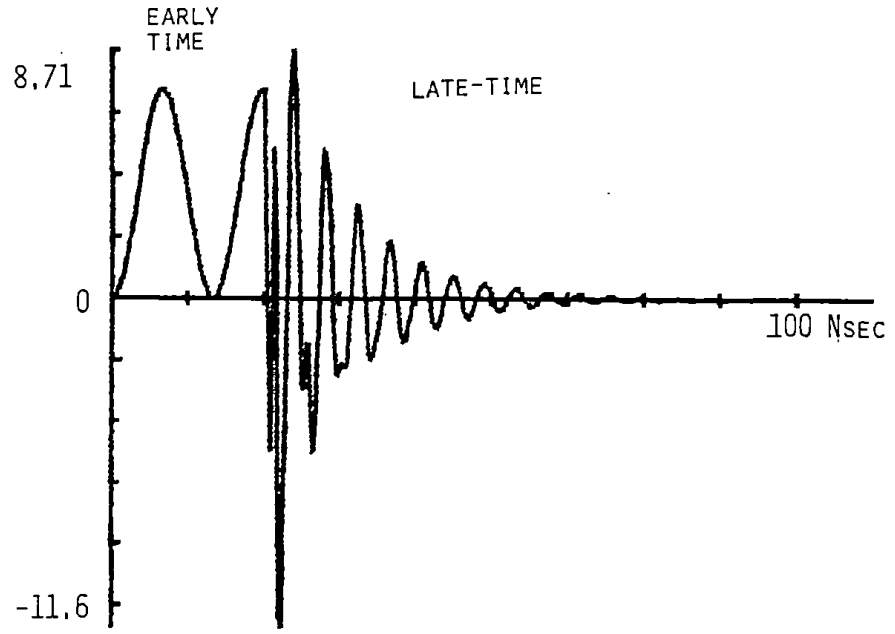

Figure 4. 6-Mode synthetic waveform (no noise).

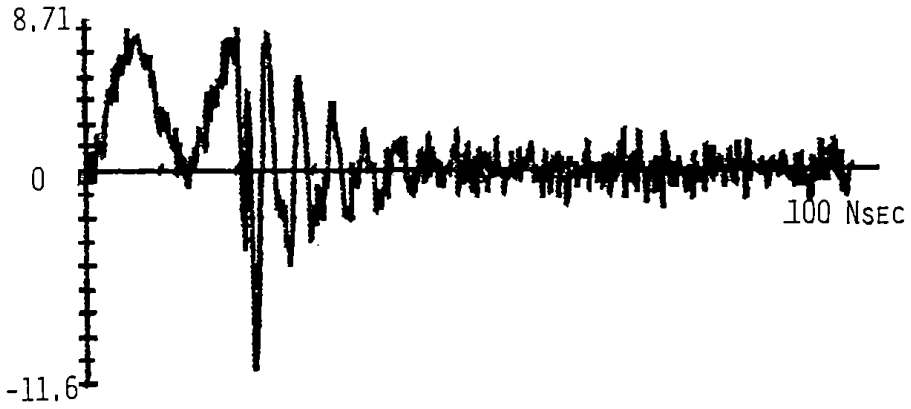

Figure 5. 6-Mode synthetic waveform (10 dB SNR).

The results of the tests for the analog-based RAF are displayed in Table 2, where the late-time signal energies are tabulated. In following each vertical column, the exact RAF should ideally display the lowest output energy. The result in the last column and second row indicates that for the case of six pole-pair filters, the 5% displaced pole-pair RAF yields a smaller signal energy than does the exact RAF. The source of this error is alluded to by the output waveform for the exact $N = 6$ RAF, as shown in Fig. 6. Ideally, the late-time data should

be very close to zero for this case. The observed late-time residual is due to high-frequency amplification of small round-off errors. Recall, that in implementing the differential equation approach, the digital FFT of the sampled $y(t)$ is multiplied at discrete frequency points by the analog $K(\omega)$ in (12), followed by an inverse FFT to obtain the output waveform. Round-off errors in the FFT (in say the 12-th decimal place) are amplified by the high-order (12-th order in this case) all-zero filter characteristic polynomial in $K(\omega)$. The nature of this error has been confirmed by extensive tests for various orders of differentiation. The precise spectral characteristics of the roundoff error is hardware and software dependent. In any case, simulation of *high-order* analog differentiation using discrete FFT methods appears to be unworkable without excessive wordlength requirements on the arithmetic computations involved.

	RAF Pole-Pairs			
	1	2	4	6
Exact	1.5E-2	6.04E-5	2.43E-9	6.38E-16
5 % Shift	2.5E-2	1.50E-4	3.65E-9	3.29E-16
10 % Shift	2.0E-1	1.49E-3	1.50E-8	6.94E-16

Table 2. Analog-based RAF late-time energy (Noiseless case).

	RAF Pole-Pairs			
	1	2	4	6
Exact	7.9E-24	2.16E-23	7.32E-23	1.17E-16
5 % Shift	1.0E-3	5.95E-5	3.29E-5	9.90E-2
10 % Shift	7.0E-3	3.09E-4	3.97E-4	1.55

Table 3. Digital FIR RAF late-time energy (Noiseless synthetic signal case).

Turning now to the digital FIR realization of the RAF, the tests were repeated using the same clean and noisy (10 dB SNR) synthetic signals. The unit sample response of the $N = 6$ digital RAF is shown in Fig. 7, where the horizontal scale has been greatly expanded to show the initial 13 non-zero values. The output of this exact RAF, as is shown in Fig. 8, displays virtually zero late-time response, without the need for any smoothing. However, a very large high frequency oscillation occurs near T_o. The level of this oscillation is so large that extensive clipping appears in the figure; a reduced dynamic range has been employed so that the late-time level can be seen. The synthetic $y(t)$ has discontinuous derivatives at $t = T_o$, and these are amplified by the high-frequency asymptotic behavior of $K(\omega)$, which is shown in Fig. 9. Since the proper RAF filter exactly cancels the matched noiseless late-time signal there is no noticeable effect except near T_o. There are 13 (i.e., $2N + 1$) data points being affected. Aside from the anomaly near T_o, the late-time energy results provide consistently accurate identifications of the synthetic signals, as is summarized in Table 3.

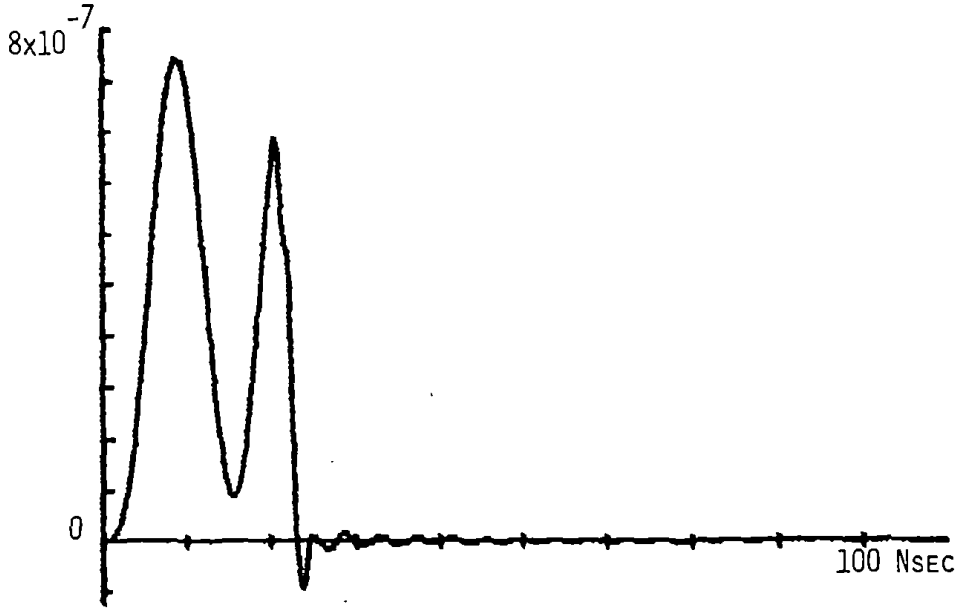

Figure 6. Output of exact 6-mode analog RAF.

RAF, the tests were repeated
ietic signals. The unit sample
. 7, where the horizontal scale
on-zero values. The output of
ually zero late-time response,
y large high frequency oscilla-
o large that extensive clipping
as been employed so that the
s discontinuous derivatives at
iency asymptotic behavior of
RAF filter exactly cancels the
ceable effect except near T_o.
ted. Aside from the anomaly
tently accurate identifications
3.

100 NSEC

analog RAF.

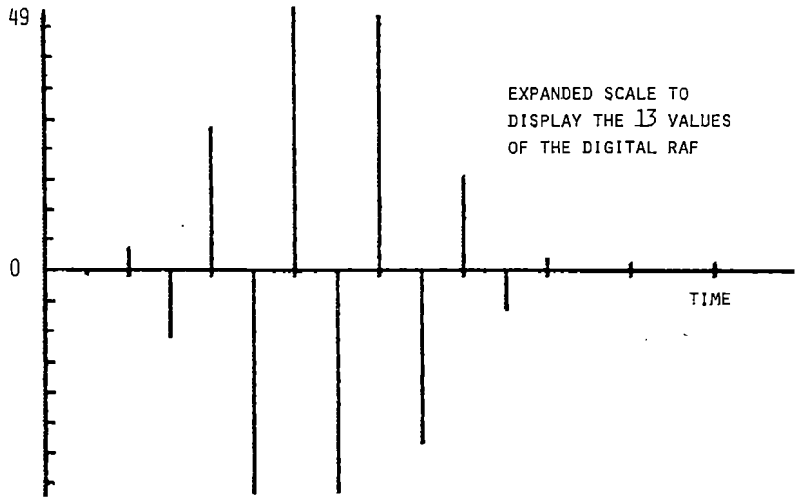

Figure 7. Unit sample response of digital 6-mode RAF.

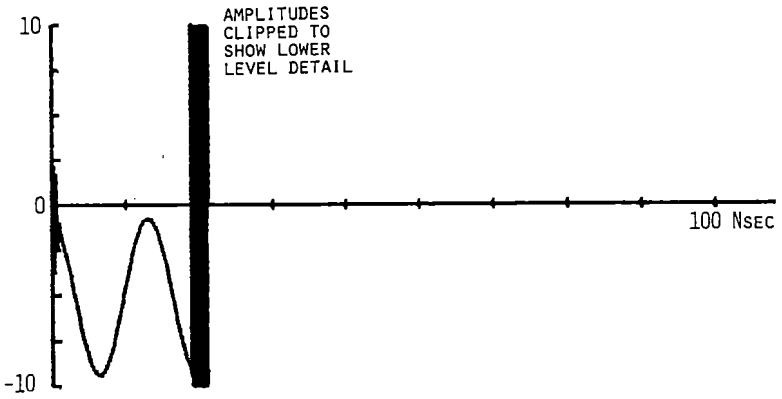

Figure 8. Output of exact 6-mode digital RAF (no noise).

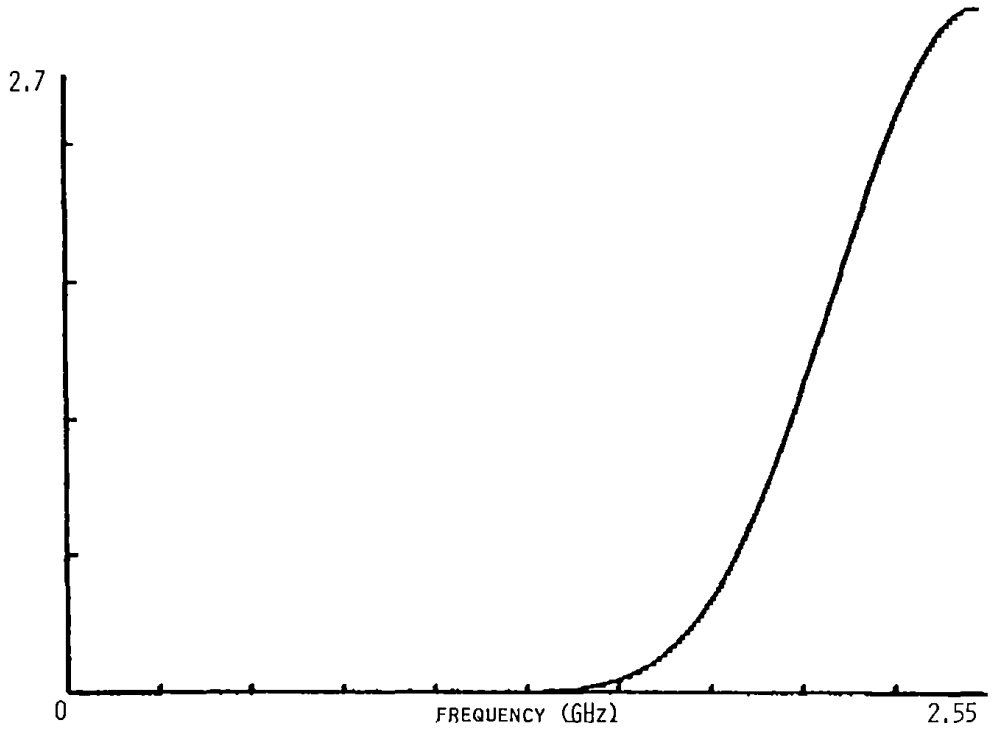

Figure 9. Spectral magnitude of digital 6-mode RAF.

For the case of 10 dB SNR, an additional Gaussian-shaped smoothing function was used to reduce the high-frequency content of the additive noise. The output for the exact RAF is shown in Fig. 10 and the late-time signal energies are displayed in Table 4. Note, that with the smoothing function convolution, the large oscillation near T_o has disappeared. The improvement of performance accompanying the increase of the number of pole-pairs ($N = 1, 2, 4$ and 6) in the RAF can be seen by comparing energy ratios in each column of Table 4.

	RAF Pole-Pairs			
	1	2	4	6
Exact	630.4	2.80E-2	1.13E-4	6.43E-6
5 % Shift	773.9	4.20E-2	2.86E-4	5.46E-5
10 % Shift	940.9	6.20E-2	7.07E-4	1.99E-4

Table 4. Digital FIR RAF late-time energy (10 dB SNR synthetic signal case).

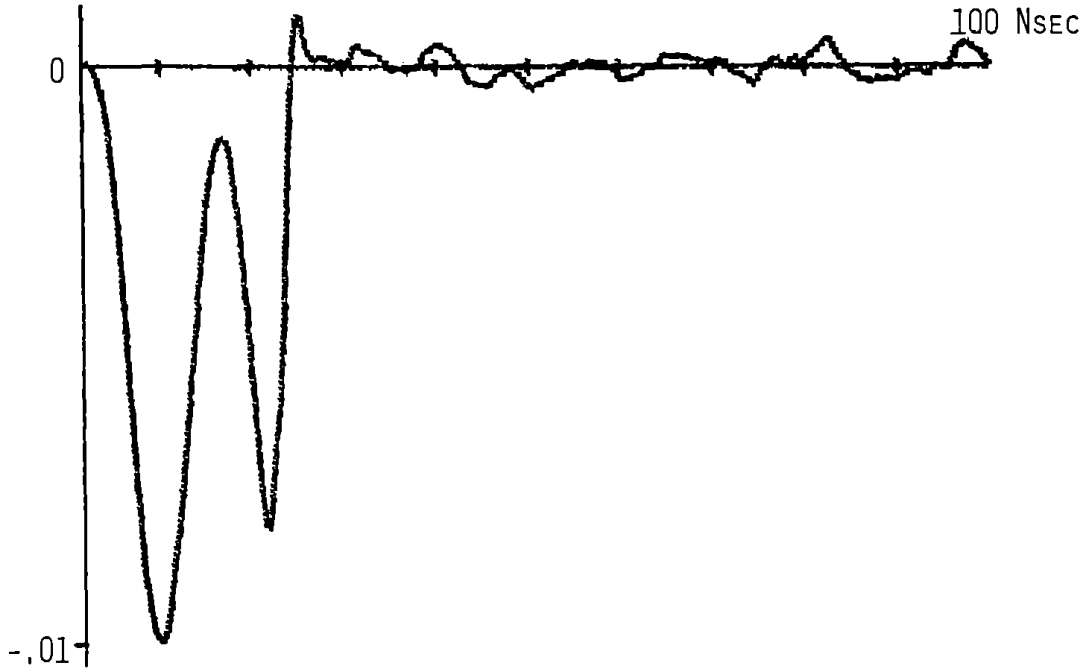

Figure 10. Output of exact 6-mode digital RAF (10 dB SNR).

The next stage of concept validation for digital RAF-based NCTR employed numerically computed electromagnetic scattering signatures from thin conducting wires, where both the complex pole values and the scattering response could be obtained to a high accuracy. Thin-wire scattering is depicted in Fig. 11, where a 1 V/m peak Gaussian-shaped incident E-field pulse, having a 10% pulse duration of 2 nsec, arrives at an angle of incidence, θ_i. The incident field is linearly polarized, with the E-field parallel to the plane of incidence. Three wire targets, having lengths of 0.9 m, 1.0 m and 1.1 m were considered, where the length to diameter ratio was 100 in each case. A *single* RAF was constructed for each target and was then used for all incident and scattering angles to demonstrate its aspect independence.

A time-domain thin-wire integral equation computer program was written, and extensively tested, following the method of Sayre and Harrington, [14]. An example far-zone scattered field waveform for the 1 meter thin-wire, with $\theta_i = \theta_s = 90°$, is shown in Fig. 12. The magnitude of the associated frequency spectrum is displayed in Fig. 13, where the resonant peaks are indicative of the presence of individual natural modes. These resonances are associated with complex poles in the first layer, adjacent to the $j\omega$ axis. For the case of broadside 90° incidence, only the symmetric current modes, having odd integer mode indices, are excited. For other incident angles, the antisymmetric modes were also present. The abrupt spectral rolloff beyond the $n = 5$ mode is due to the spectral bandwidth of the incident Gaussian-shaped waveform.

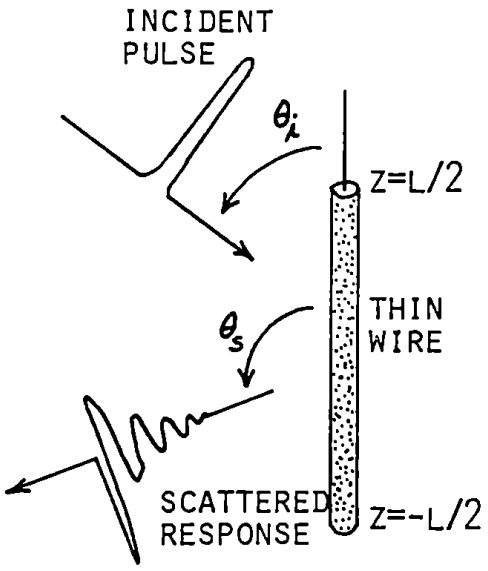

Figure 11. Thin-wire scattering geometry.

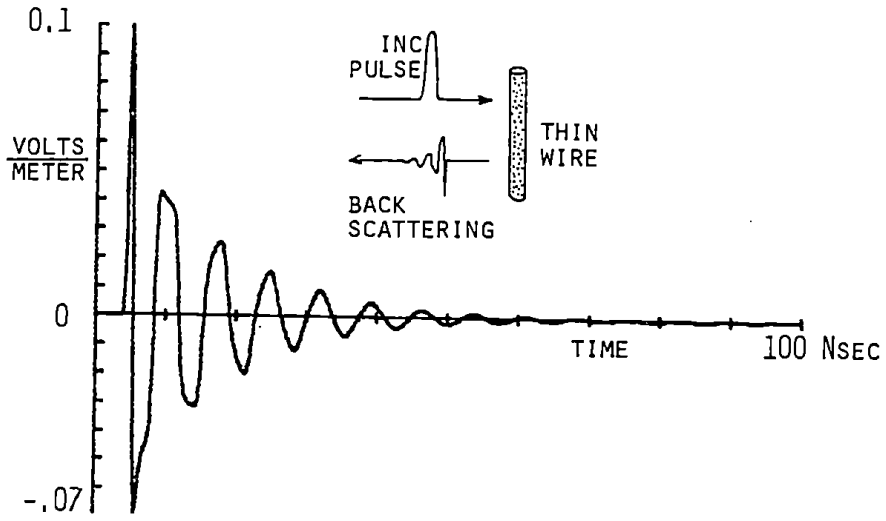

Figure 12. Thin-wire scattered field signature $\theta_i = \theta_s = 90^o$.

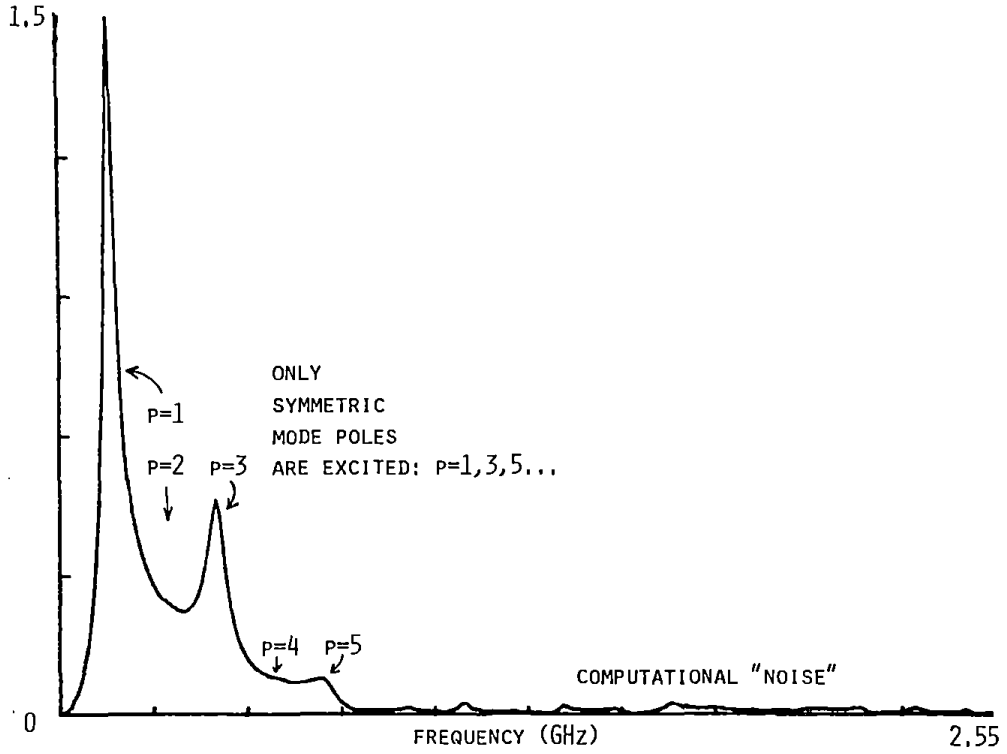

Figure 13. Scattered field spectral magnitude $\theta_i = \theta_s = 90°$.

Resonant filters which canceled the first seven pole-pairs for each of the three thin-wires were implemented, using the digital FIR design technique. Pole values were extrapolated from parameterized plots in the work of Tesche, [15], with an accuracy of about 3 decimal places. Example RAF outputs are displayed in Fig. 14, for the case of a 10 dB SNR waveform from the 1 meter wire, with $\theta_i = 90°$ and $\theta_s = 45°$. The late-time energy results are summarized in Tables 5 and 6 for the respective cases of no additive noise and 10 dB SNR additive noise. For the sake of brevity, these tables only display the results of RAF operations on the scattered waveforms from the 1 meter wire. Equally good results were obtained in processing the waveforms from the other two wires; the matched RAF consistently provided the lowest late-time signal energy, independent of bistatic aspects on the target. A special double-Gaussian smoothing function was employed with the noisy data to reduce both high *and* low frequency noise content. This smoothing function is the sum of two colocated Gaussian functions having opposite polarity and different standard deviations. The resultant function has zero mean. Adjustment of the two independent standard deviations allows tailoring of the frequency filtering characteristics at both the high and low range. As is apparent, consistently good identifications can be made even with a relatively low fidelity scattered signal, at least in the case of thin-wire targets.

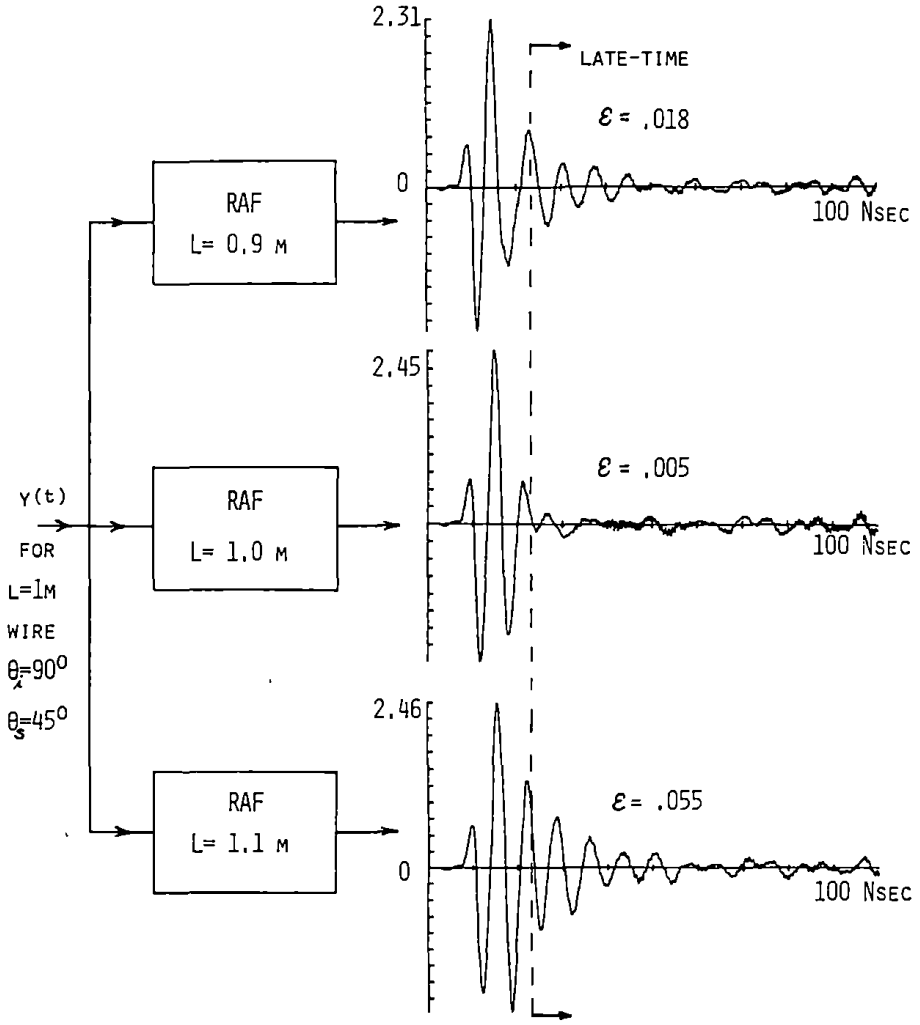

Figure 14. RAF outputs for $L = 1$ m wire scattered signal (10 dB SNR).

	Bistatic θ_i/θ_s (degrees)			
	90/90	90/45	45/135	45/45
$L = 0.9$ m	4.24E-15	1.87E-15	1.33E-15	9.35E-16
$L = 1.0$ m	7.99E-18	3.00E-18	1.90E-9	2.04E-18
$L = 1.1$ m	1.30E-17	5.38E-18	3.74E-18	2.82E-18

Table 5. Digital FIR late-time energy (Noiseless thin-wire I.E. case).

	Bistatic θ_i/θ_s (degrees)			
	90/90	90/45	45/135	45/45
$L = 0.9$ m	.045	.018	.012	.014
$L = 1.0$ m	.019	.005	.005	.008
$L = 1.1$ m	.122	.055	.028	.038

Table 6. Digital FIR late-time energy (10 dB SNR thin-wire I.E. case).

	Wire Length for Data		
	9 cm	10 cm	11 cm
RAF			
$L =$ 9 cm	2.53	12.92	53.95
$L =$10 cm	15.88	2.89	10.97
$L =$11 cm	41.07	17.31	3.79

Table 7. Digital FIR late-time energy (Measured thin-wire broadside backscatter).

The final evaluation of the RAF concept was through use of experimental broadside back-scattering signatures of copper wires having lengths of 9 cm, 10 cm and 11 cm, with a common diameter of 0.24 cm. Transient scattering data was obtained from the Transient Electromagnetic Scattering Laboratory at the Naval Postgraduate School, [16]. An example scattering signature and its corresponding spectral magnitude (for the 10 cm wire) are respectively shown in Figs. 15 and 16. The scattering responses are due to a double-Gaussian excitation. Because of the filtering that was used in synthesizing the double-Gaussian response from the measured data, it was not necessary to perform further smoothing. Only three significant pole-pairs are present in the data, as evidenced by their spectral behavior. These poles were estimated from [15]. The measured broadside backscattering

signatures of each of the three wires was then filtered by each of the three RAFs, with the late-time energy results being shown in Table 7. The consistently low energies provided by the proper RAFs appear as the diagonal values in this table. These results, although hardly comprehensive, provide a demonstration of the aspect independent nature of this method which is based upon experimental data.

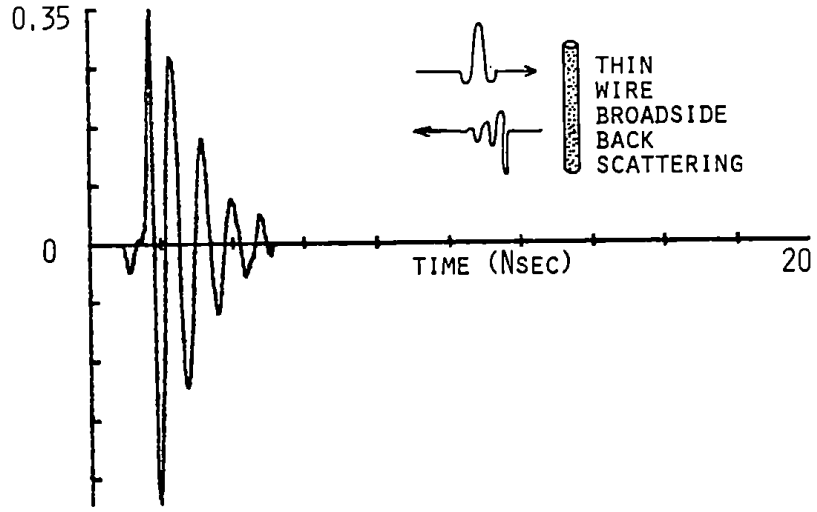

Figure 15. Measured transient scattering response of $L = 10$ cm wire.

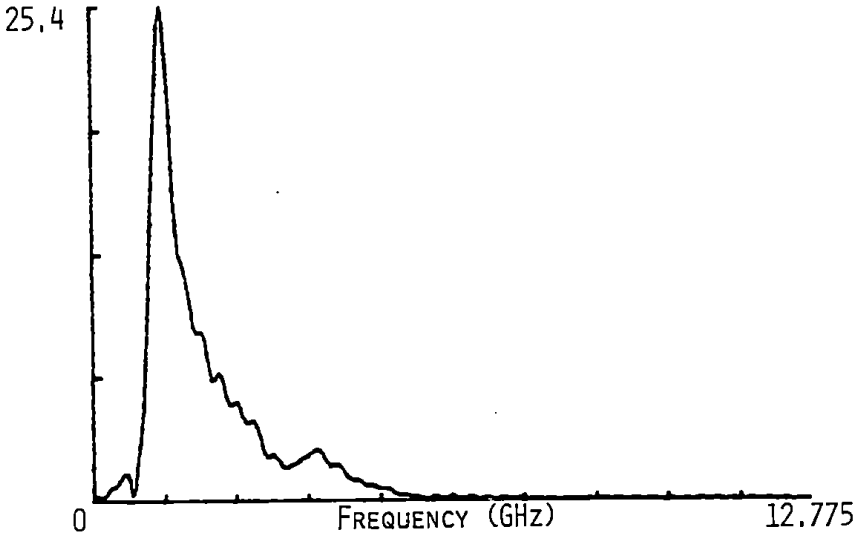

Figure 16. Spectral magnitude of measured scattering response.

CONCLUSION

A new class of resonance annihilation filters for aspect-independent NCTR, which makes use of simple digital FIR filters, has been described and tested on a limited basis using synthetic waveforms, integral equation computations and measured data. An earlier concept, based upon analog differential operators, was also described and then shown to fail due to high-level amplification of otherwise insignificant roundoff errors in the digital implementation.

Future work will involve further refinements and more comprehensive validations of the RAF method. An initial endeavor will be to conduct a performance comparison with the alternate "E-pulse" method, which has been developed by Chen and others, [9]. This cooperative effort will be an initial step towards the development of systematic digital design methods to optimize the RAF performance for realistic cases of transient scattering. Such optimization will address several issues, including moderate and low "Q" target signatures, which have more rapidly damped natural modes than those of thin-wires.

An additional concern is the tradeoff of system bandwidth reduction for reduced decision reliability. This will be considered as part of a more general effort which seeks to quantify the expected error probabilities as a function of (1) spectral characteristics, (2) SNR and (3) target ensemble. This latter consideration will be highly significant since a target ensemble which has elements whose dominant poles are close to those of other elements will be more difficult to consistently identify. Another aspect of the selectivity issue concerns multiple configurations of a single target type due, for instance, to variable wing sweep and stores. The viability of the resonance annihilation method for real-world NCTR may ultimately prove insufficient for stand-alone aspect-independent identification. On the other hand, the late-time data set may be highly useful when augmented by aspect-dependent imaging methods, which primarily employ the early-time signal.

ACKNOWLEDGMENTS

This work was supported by the Electronics Division of the Office of Naval Research under contract N00014-81-WR-10226. The author is grateful to Captain James B. Dunavin (USAF), Captain King W. Jean (Canadian Forces) and Lieutenant Commander Brent W. McDaniel (USN) for their assistance.

The Editor thanks C. E. Baum, D. Nyquist, L. W. Pearson, and one anonymous Reviewer for reviewing the paper.

REFERENCES

1. Mains, R. H., and D. L. Moffatt, "Complex natural resonances of an object in detection and discrimination," TR-3424-1, Ohio State University, Electroscience Laboratory, Columbus, OH, June 1974.
2. Baum, C. E., "On the singularity expansion method for the solution of electromagnetic interaction problems," AFWL Interaction Note 88, Dec. 11, 1971.
3. Tesche, F. M., "The far-field response of a step-excited linear antenna using SEM," *IEEE Trans. Antennas and Propagat.*, Vol. AP–23, 834–838, Nov. 1975.
4. Morgan, M. A., "Singularity expansion representations for fields and currents in

electromagnetic scattering," *IEEE Trans. Antennas Propagat.*, Vol. AP–32, 466–473, May 1984.
5. Pearson, L. W., "A note on the representation of scattered fields as a singularity expansion," *IEEE Trans. Antennas Propagat.*, Vol. AP–32, 520–523, May 1984.
6. Auton, J. R., T. L. Larry, and M. L. Van Blaricum, "Radar target identification and characterization using natural resonance extraction," Final Report on ONR Contract N00014-82-C-0079, September 1984.
7. Kennaugh, E. M., "The K-pulse concept," *IEEE Trans. Antennas Propagat.*, Vol. AP–29, March 1981.
8. Morgan, M. A., and J. B. Dunavin, "Discrimination of scatterers using natural resonance annihilation," *Abstracts of 1986 National Radio Science Meeting*, Philadelphia, PA, June 1986.
9. Chen, K. M., D. P. Nyquist, E. J. Rothwell, L. L. Webb, and B. Drachman, "Radar target discrimination by convolution of radar return with extinction-pulses and single-mode extraction signals," *IEEE Trans. Antennas and Propagat.*, Vol. AP–34, 896–904 July 1986.
10. Mittra, R., "Integral equations in transient scattering," in *Transient Electromagnetic Fields*, L. Felsen, Ed., Springer-Verlag, New York, 75–127, 1976.
11. Marin, L., "Representation of transient scattered fields in terms of free oscillations of bodies," *Proc. IEEE*, Vol. 60, 640–641, May 1972.
12. Kennaugh, E. M., and R. L. Cosgriff, "The use of impulse response in electromagnetic scattering problems," *Proceedings 1958 IRE National Convention Record*, Part I, 72–77.
13. Oppenheim, A. V., and R. W. Schafer, *Digital Signal Processing*, Prentice-Hall, Englewood Cliffs, Chap. 5, 1975,
14. Sayre, E. P., and R. F. Harrington, "Time-domain radiation and scattering by thin-wires," *Applied Science Res.*, Vol. 26, 413–444, 1972.
15. Tesche, F. M., "On the analysis of scattering and antenna problems using the singularity expansion technique," *IEEE Trans. Antennas and Propagat.*, Vol. AP–21, 53–62, Jan. 1973.
16. Morgan, M. A., "Time-domain scattering measurements," *IEEE Antennas and Propagation Newsletter*, Vol. 6, 5–9, Aug. 1984.

Michael A. Morgan received the Ph.D. from U.C. Berkeley in 1976 and has since held positions at SRI and the Univ. of Mississippi before joining the Electrical and Computer Engineering Faculty at the Naval Postgraduate School in 1979. During FY 1986 he managed the electromagnetics program at the Office of Naval Research. His interests include finite element computational electromagnetics, natural resonance scattering theory, transient scattering measurements and the control of scattering mechanisms.